

Crystal structure of racemic benserazide hydrochloride Form I, $C_{10}H_{16}N_3O_5Cl$

James A. Kaduk ^{1,2,a)} Anja Dosen ³ and Thomas N. Blanton ³

¹Illinois Institute of Technology, 3101 S. Dearborn St., Chicago, IL 60616, USA

²North Central College, 131 S. Loomis St., Naperville, IL 60540, USA

³ICDD, 12 Campus Blvd., Newtown Square, PA 19073-3273, USA

(Received 19 June 2024; accepted 24 September 2024)

The crystal structure of benserazide hydrochloride Form I has been solved and refined using synchrotron X-ray powder diffraction data and optimized using density functional theory techniques. Benserazide hydrochloride Form I crystallizes in space group $P2_1/n$ (#14) with $a = 19.22983(15)$, $b = 14.45066(10)$, $c = 4.57982(2)$ Å, $\beta = 93.6935(3)$, $V = 1270.014(15)$ Å³, and $Z = 4$ at 295 K. The crystal structure contains pairs of hydrogen-bonded benserazide cations, which are hydrogen bonded to chloride anions, resulting in chains along the c -axis. In addition, O–H...Cl, N–H...O, O–H...N, and O–H...O hydrogen bonds link the cations and anions into a three-dimensional framework. The powder pattern has been submitted to ICDD® for inclusion in the Powder Diffraction File™ (PDF®).

© The Author(s), 2024. Published by Cambridge University Press on behalf of International Centre for Diffraction Data. This is an Open Access article, distributed under the terms of the Creative Commons Attribution licence (<http://creativecommons.org/licenses/by/4.0/>), which permits unrestricted re-use, distribution and reproduction, provided the original article is properly cited.

[doi:10.1017/S0885715624000496]

Key words: benserazide, Serazide, crystal structure, Rietveld refinement, density functional theory

I. INTRODUCTION

Benserazide hydrochloride, also referred to as Serazide, is used for the management of Parkinson's disease. By itself benserazide HCl has minimal therapeutic effect, and functions in combination with administered L-DOPA (levodopa) by limiting L-DOPA decarboxylation. The L-DOPA is able to pass from the bloodstream to the brain, concentrate in the brain where L-DOPA decarboxylation can occur, resulting in the formation of dopamine which provides the desired therapeutic result. It is on the World Health Organization's List of Essential Medicines. The systematic name (CAS Registry Number 14919-77-8) is 2-amino-3-hydroxy-*N'*-(2,3,4-trihydroxybenzyl)propanehydrazide hydrochloride. A two-dimensional molecular diagram of benserazide hydrochloride is shown in Figure 1.

The preparation of benserazide hydrochloride has been described in US Patent 3,178,476 (Hegedus and Zeller, 1965; Hoffman-La Roche). Benserazide hydrochloride has several polymorphs and forms solvates easily (Jokela et al., 2015; Orion Corporation). Form I is found in commercial tablets, and Jokela et al. provide a powder diffraction pattern for it, as well as for hydrated Form VI and DMF solvate Form IX.

This work was carried out as part of a project (Kaduk et al., 2014) to determine the crystal structures of large-volume commercial pharmaceuticals, and include high-quality powder diffraction data for them in the Powder Diffraction File (Kabekkodu et al., 2024).

II. EXPERIMENTAL

Benserazide hydrochloride was a commercial reagent, purchased from Target Mol (Batch #159174), and was used as-received. The off-white powder was packed into a 0.5-mm diameter Kapton capillary and rotated during the measurement at ~2 Hz. The powder pattern was measured at 298(1) K at the BXDS-WLE Wiggler Low Energy Beamline (Leontowich et al., 2021) of the Brockhouse X-ray Diffraction and Scattering Sector of the Canadian Light Source using a wavelength of 0.819563(2) Å (15.1 keV) from 1.6 to 75.0° 2θ with a step size of 0.0025° and a collection time of 3 min. The high-resolution powder diffraction data were collected using eight Dectris Mythen2 X series 1 K linear strip detectors. NIST SRM 660b LaB₆ was used to calibrate the instrument and refine the monochromatic wavelength used in the experiment.

The pattern was indexed with N-TREOR implemented in EXPO2014 (Altomare et al., 2013) on a primitive monoclinic unit cell with $a = 19.23310$, $b = 14.45764$, $c = 4.58238$ Å, $\beta = 93.672^\circ$, $V = 1271.6$ Å³, and $Z = 4$. The suggested space group was $P2_1/n$, which was confirmed by successful solution and refinement of the structure, so apparently what was purchased was a racemate. A reduced cell search of the Cambridge Structural Database (Groom et al., 2016) yielded 5 hits, but no benserazide derivatives.

The structure was solved by direct methods as implemented in EXPO2014 (Altomare et al., 2013), using the COVMAP option. A few atom types had to be reassigned manually. The initial hydrogen atom positions were calculated using Mercury (Macrae et al., 2020). Analysis of potential N–H...Cl hydrogen bonds suggested that N7 was protonated,

^{a)} Author to whom correspondence should be addressed. Electronic mail: kaduk@polycrystallography.com



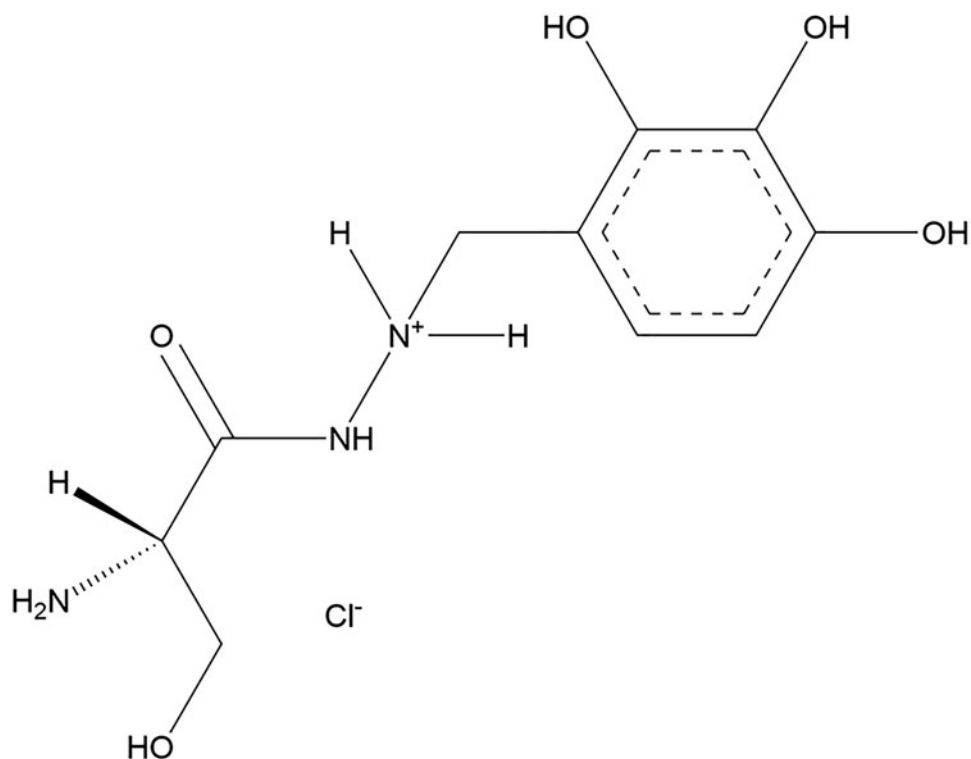


Figure 1. The two-dimensional representation of the molecular structure of benserazide hydrochloride.

so H35 was added there. However, the density functional theory (DFT) calculation moved H35 to N9, so the final refinement was started from the DFT-optimized structure.

Rietveld refinement was carried out with GSAS-II (Toby and Von Dreele, 2013). Only the 3.6–65.0° portion of the pattern was included in the refinements ($d_{\min} = 0.763 \text{ \AA}$). All non-H bond distances and angles were subjected to restraints, based on a Mercury/Mogul Geometry Check (Bruno et al.,

2004; Sykes et al., 2011). The Mogul average and standard deviation for each quantity were used as the restraint parameters. The benzene ring was restrained to be planar. The restraints contributed 1.3% to the overall χ^2 . The hydrogen atoms were included in calculated positions, which were recalculated during the refinement using Materials Studio (Dassault Systèmes, 2023). The U_{iso} of the heavy atoms were grouped by chemical similarity. The chloride anion Cl1 was refined

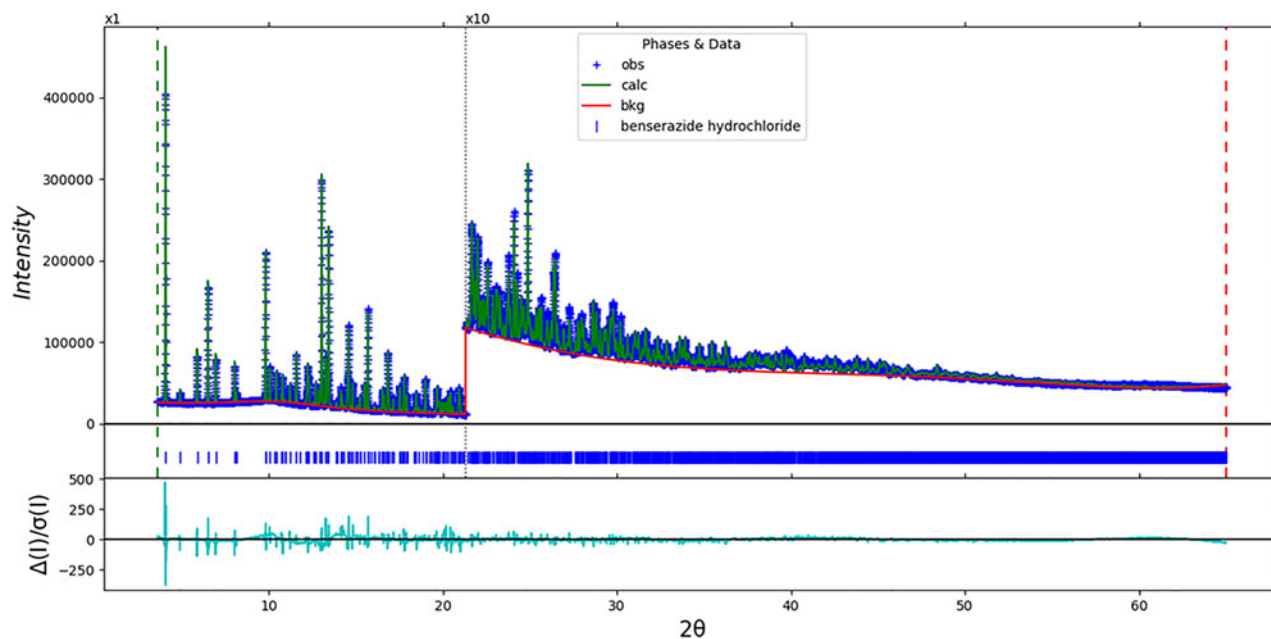


Figure 2. The Rietveld plot for the refinement of benserazide hydrochloride Form I. The blue crosses represent the observed data points, and the green line is the calculated pattern. The cyan curve is the normalized error plot, and the red line is the background curve. The vertical scale has been multiplied by a factor of 10x for $2\theta > 21.3^\circ$.

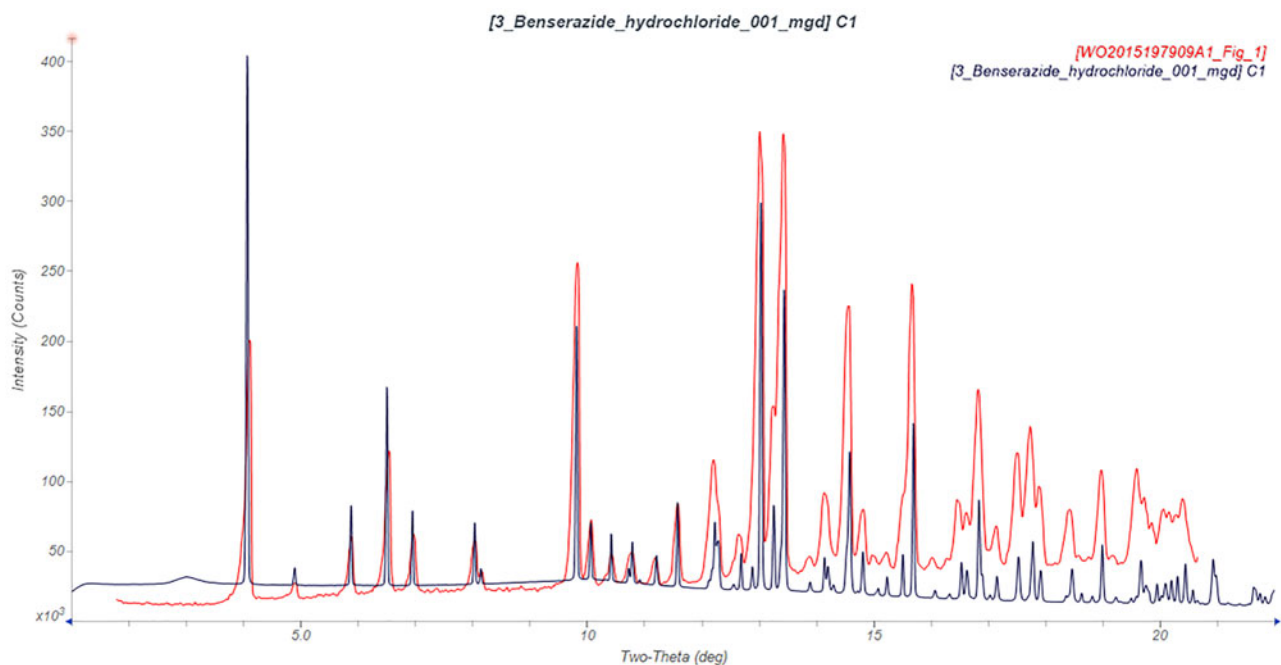


Figure 3. Comparison of the synchrotron pattern of benserazide hydrochloride (black) to that of Form I reported by Jokela et al. (2015; red). The literature pattern (measured using Cu K_{α} radiation) was digitized using UN-SCAN-IT (Silk Scientific, 2013) and converted to the synchrotron wavelength of 0.819563(2) Å using JADE Pro (MDI, 2024). Image generated using JADE Pro (MDI, 2024).

anisotropically. The U_{iso} for the H atoms were fixed at $1.3 \times$ the U_{iso} of the heavy atoms to which they are attached. The peak profiles were described using the generalized microstrain model (Stephens, 1999). The background was modeled using a 6-term shifted Chebyshev polynomial, with a peak at 10.35° to model the scattering from the Kapton capillary and any amorphous component.

The final refinement of 93 variables using 24,561 observations and 43 restraints yielded the residual $R_{\text{wp}} = 0.0469$. The largest peak (0.66 Å from C18) and hole (1.21 Å from C12) in the difference Fourier map were $0.92(21)$ and $-0.93(21) e\text{Å}^{-3}$, respectively. The final Rietveld plot is shown in Figure 2. The largest features in the normalized error plot are in the shapes of some of the low-angle peaks.

The crystal structure of benserazide hydrochloride Form I was optimized (fixed experimental unit cell) with density functional techniques using VASP (Kresse and Furthmüller,

1996) through the MedeA graphical interface (Materials Design, 2024). The calculation was carried out on 32 cores of a 144-core (768 GB memory) HPE Superdome Flex 280 Linux server at North Central College. The calculation used the GGA-PBE functional, a plane wave cutoff energy of 400.0 eV, and a k -point spacing of 0.5 Å^{-1} leading to a $3 \times 1 \times 3$ mesh, and took ~ 9.3 h. Single-point DFT calculations (fixed experimental cell) and population analysis were carried out using CRYSTAL23 (Erba et al., 2023). The basis sets for the H, C, N, and O atoms in the calculation were those of Gatti et al. (1994), and that for Cl was that of Peintinger et al. (2013). The calculations were run on a 3.5 GHz PC using 8 k -points and the B3LYP functional, and took ~ 1.7 h.

III. RESULTS AND DISCUSSION

The powder pattern of this study is similar enough to that reported by Jokela et al. (2015) to conclude that they represent the same material (Figure 3), and thus our sample is Form I. The root-mean-square (rms) Cartesian displacement of the non-H atoms in the Rietveld-refined and VASP-optimized molecules is 0.118 Å (Figure 4). The agreement is within the normal range for correct structures (van de Streek and Neumann, 2014). The difference in the absolute positions of the chloride anions is 0.606 Å. The asymmetric unit is illustrated in Figure 5. The remaining discussion will emphasize the VASP-optimized structure.

All of the bond distances and bond angles, and all but one of the torsion angles fall within the normal ranges indicated by a Mercury/Mogul Geometry Check (Macrae et al., 2020). No hits were found for the C17–N7–N9–C16 torsion angle; this is an unusual group of atoms. Quantum chemical geometry optimization of the isolated molecules (DFT/B3LYP/6-31G*/water) using Spartan '24 (Wavefunction, 2023) indicated that the cation is close to a local minimum-energy

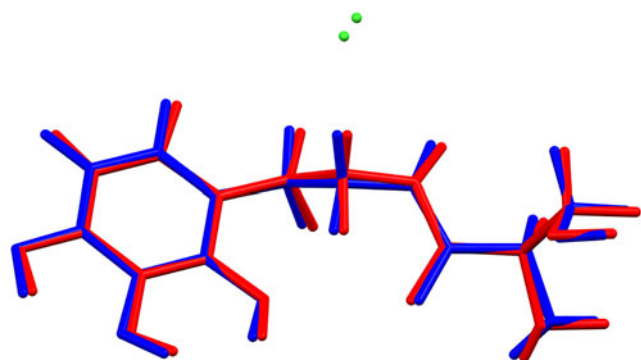


Figure 4. Comparison of the Rietveld-refined (red) and VASP-optimized (blue) structures of the cation in benserazide hydrochloride Form I. The rms Cartesian displacement is 0.117 Å. Image generated using Mercury (Macrae et al., 2020).

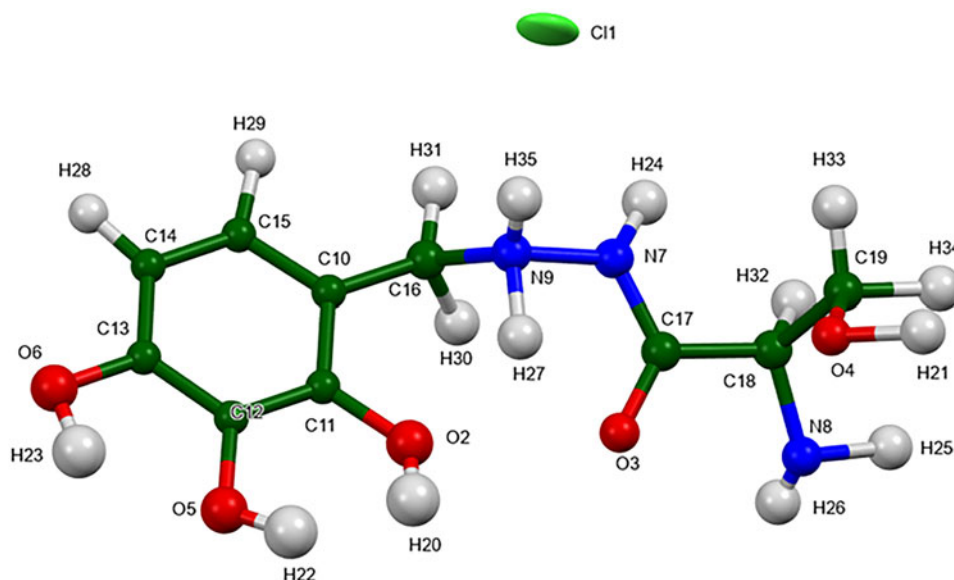


Figure 5. The asymmetric unit of benserazide hydrochloride Form I, with the atom numbering. The atoms are represented by 50% probability spheroids/ellipsoids. Image generated using Mercury (Macrae et al., 2020).

conformation (rms displacement = 0.453 Å). The global minimum-energy conformation (MMFF) is much more compact, showing that intermolecular interactions are important to determining the solid-state conformations.

The crystal structure (Figure 6) contains pairs of hydrogen-bonded benserazide cations, which are hydrogen bonded

to chloride anions. Analysis of the contributions to the total crystal energy of the structure using the Forcite module of Materials Studio (Dassault Systèmes, 2023) indicates that torsion, angle, and bond distortion terms contribute significantly to the intramolecular energy. The intermolecular energy is dominated by van der Waals repulsions and electrostatic

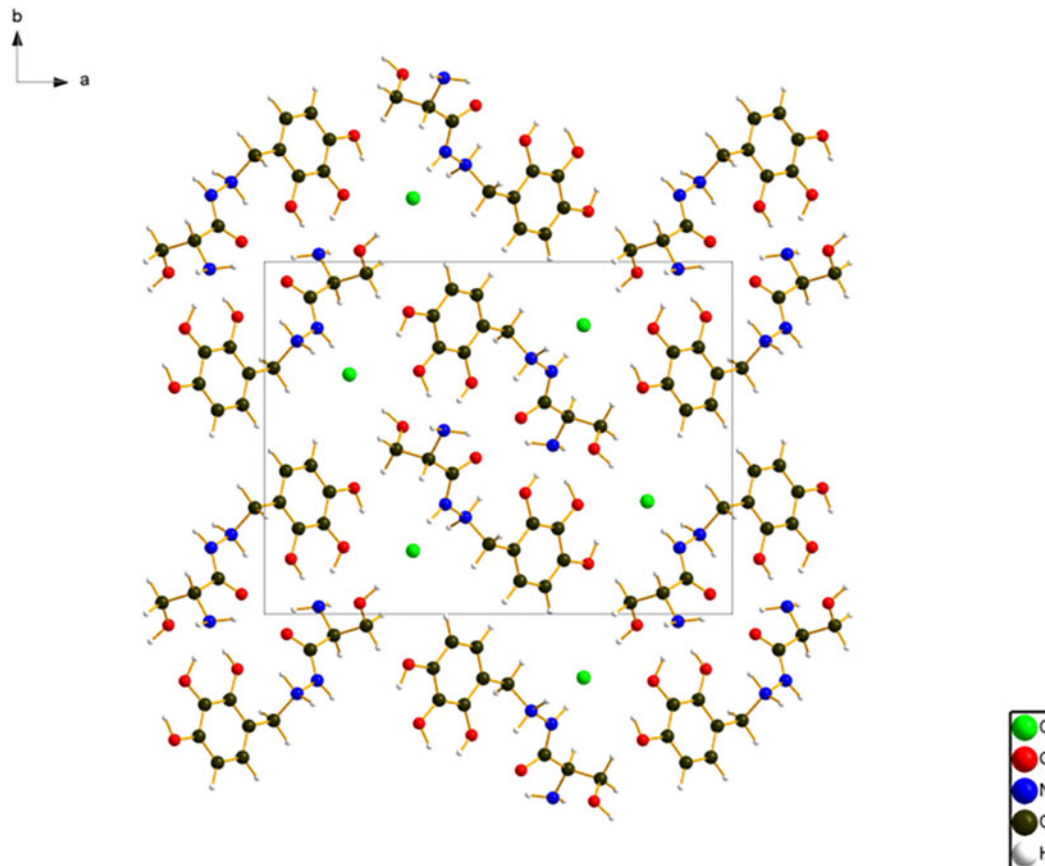


Figure 6. The crystal structure of benserazide hydrochloride Form I, viewed down the *c*-axis. Image generated using Diamond (Crystal Impact, 2023).

TABLE I. Hydrogen bonds (CRYSTAL23) in benserazide hydrochloride Form I.

H-Bond	D-H (Å)	H...A (Å)	D...A (Å)	D-H...A (°)	Overlap (<i>e</i>)	E (kcal mol ⁻¹)
N9-H35...Cl1	1.075	1.976	3.018	162.5	0.106	
N7-H24...Cl1	1.055	2.001	3.015	160.4	0.096	
O4-H21...Cl1	0.990	2.140	3.121	170.5	0.060	
O6-H23...Cl1	0.989	2.793	3.687	150.7	0.023	
O6-H23...O5	0.989	2.031 ^a	2.622	116.2	0.024	
N9-H27...O2	1.053	1.883 ^a	2.721	133.9	0.048	5.1
N9-H27...O3	1.053	2.117 ^a	2.668	110.0	0.032	4.1
N8-H26...O3	1.026	2.317	3.285	156.8	0.019	3.2
N8-H25...O4	1.035	1.816	2.818	161.8	0.056	5.5
O5-H22...N8	11.028	1.647	2.658	166.5	0.078	
O2-H20...N8	0.987	2.238	3.166	156.3	0.028	
O2-H20...O3	0.987	2.472	3.087	120.1	0.014	6.5
C14-H28...Cl1	1.091	3.071	4.105	158.4	0.019	
C18-H32...Cl1	1.106	3.006	3.838	132.3	0.011	
C19-H33...O6	1.100	2.430	3.333	138.3	0.014	

^aIntramolecular.

attractions, which in this force-field-based analysis include hydrogen bonds. The hydrogen bonds are better discussed using the results of the DFT calculation.

Hydrogen bonds are prominent in the crystal structure (Table I; Figure 7). Both N atoms of the central hydrazide linkage form strong N-H...Cl hydrogen bonds to the anion. The Mulliken overlap populations suggest that the hydrogen bonds from the cationic N7 and neutral N9 are of comparable strength. These N-H...Cl hydrogen bonds link the cations and anions into chains along the *c*-axis. The two hydroxyl groups O4 and O6 also form hydrogen bonds to the anion. The cationic N9 forms two intramolecular N-H...O hydrogen bonds, and the amino group N8 acts as a donor in two additional N-H...O hydrogen bonds. The hydroxyl groups O2

and O5 act as donors in O-H...N hydrogen bonds to the amino groups N8. The hydroxyl group O2 participates in an intermolecular O-H...O hydrogen bond to the carbonyl group O3. The energies of the N-H...O hydrogen bonds were calculated using the correlation of Wheatley and Kaduk (2019), and O-H...O hydrogen bonds were calculated using the correlation of Rammohan and Kaduk (2018). The result of these classical hydrogen bonds is a three-dimensional hydrogen bond network. Non-classical C-H...Cl and C-H...O hydrogen bonds also contribute to the lattice energy.

The volume enclosed by the Hirshfeld surface of benserazide hydrochloride Form I (Figure 8; Hirshfeld, 1977; Spackman et al., 2021) is 310.59 Å³, 97.82% of the unit cell volume. The packing density is thus fairly typical. The only

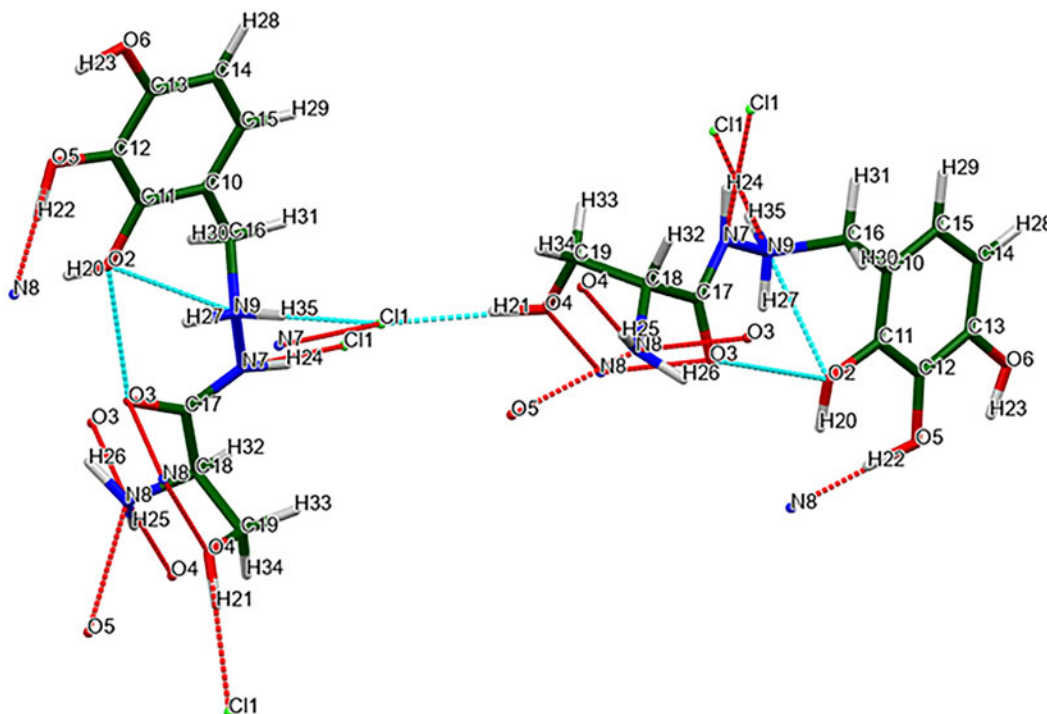


Figure 7. The hydrogen bonds (red and cyan dashed lines) in benserazide hydrochloride Form I. The cyan bonds are with a single asymmetric unit. Image generated using Mercury (Macrae et al., 2020).

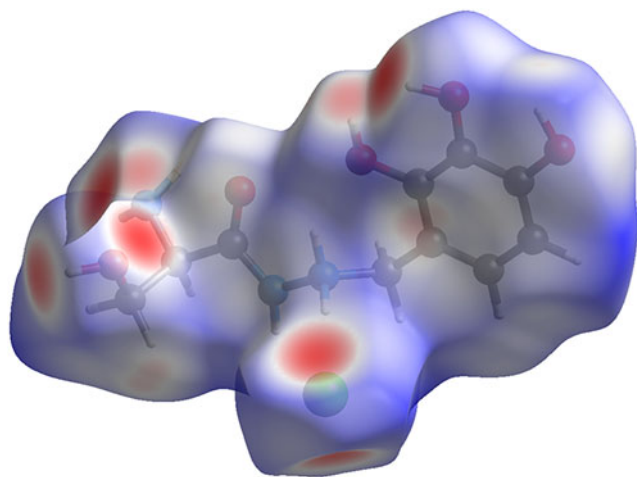


Figure 8. The Hirshfeld surface of benserazide hydrochloride Form I. Intermolecular contacts longer than the sums of the van der Waals radii are colored blue, and contacts shorter than the sums of the radii are colored red. Contacts equal to the sums of radii are white. Image generated using CrystalExplorer (Spackman et al., 2021).

significant close contacts (red in Figure 8) involve the hydrogen bonds. The volume/non-hydrogen atom is smaller than normal, at 16.7 \AA^3 .

The Bravais–Friedel–Donnay–Harker (Bravais, 1866; Friedel, 1907; Donnay and Harker, 1937) morphology suggests that we might expect needle morphology for benserazide hydrochloride Form I (Figure 9), with $\langle 001 \rangle$ as the long axis (as expected from the anisotropy of the lattice parameters). A second-order spherical harmonic model was included in the refinement. The texture index was 1.002(0), indicating that

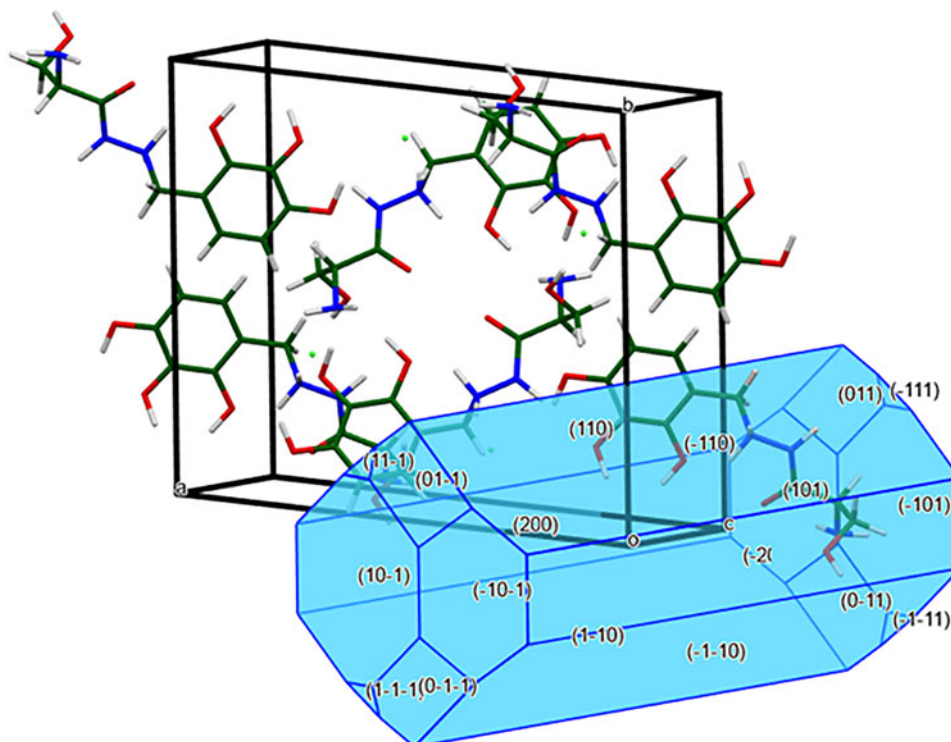


Figure 9. Bravais–Friedel–Donnay–Harker morphology for benserazide hydrochloride Form I. The long axis of the needle is the c -axis.

preferred orientation was insignificant in this rotated capillary specimen.

IV. DEPOSITED DATA

The powder pattern of benserazide hydrochloride Form I from this synchrotron data set has been submitted to ICDD for inclusion in the Powder Diffraction File. The Crystallographic Information Framework (CIF) files containing the results of the Rietveld refinement (including the raw data) and the DFT geometry optimization were deposited with the ICDD. The data can be requested at pdj@icdd.com.

ACKNOWLEDGEMENTS

Part or all of the synchrotron data collection described in this paper was performed at the Canadian Light Source, a national research facility of the University of Saskatchewan, which is supported by the Canada Foundation for Innovation (CFI), the Natural Sciences and Engineering Research Council (NSERC), the Canadian Institute of Health Research (CIHR), the Government of Saskatchewan, and the University of Saskatchewan. This work was partially supported by the International Centre for Diffraction Data. We thank Adam Leontowich for his assistance in the synchrotron data collection and Megan Rost (ICDD) for laboratory data collection before the gepirone specimen was sent to CLS.

CONFLICTS OF INTEREST

The authors have no conflicts of interest to declare.

REFERENCES

- Altomare, A., C. Cuocci, C. Giacobozzo, A. Moliterni, R. Rizzi, N. Corriero, and A. Falcicchio. 2013. "EXPO2013: A Kit of Tools for Phasing Crystal Structures from Powder Data." *Journal of Applied Crystallography* 46: 1231–35.
- Bravais, A. 1866. *Etudes Cristallographiques*. Gauthier Villars.
- Bruno, I. J., J. C. Cole, M. Kessler, J. Luo, W. D. S. Motherwell, L. H. Purkis, B. R. Smith, R. Taylor, R. I. Cooper, S. E. Harris, and A. G. Orpen. 2004. "Retrieval of Crystallographically-Derived Molecular Geometry Information." *Journal of Chemical Information and Computer Sciences* 44: 2133–44.
- Crystal Impact. 2023. *Diamond V. 5.0.0*. Crystal Impact - Dr. H. Putz & Dr. K. Brandenburg.
- Dassault Systèmes. 2023. *BIOVIA Materials Studio 2024*. BIOVIA.
- Donnay, J. D. H., and D. Harker. 1937. "A New Law of Crystal Morphology Extending the Law of Bravais." *American Mineralogist* 22: 446–67.
- Erba, A., J. K. Desmarais, S. Casassa, B. Civalleri, L. Donà, I. J. Bush, B. Searle, L. Maschio, L.-E. Daga, A. Cossard, C. Ribaldone, E. Ascrizzi, N. L. Marana, J.-P. Flament, and B. Kirtman. 2023. "CRYSTAL23: A Program for Computational Solid State Physics and Chemistry." *Journal of Chemical Theory and Computation* 19: 6891–932. doi:10.1021/acs.jctc.2c00958.
- Friedel, G. 1907. "Etudes sur la loi de Bravais." *Bulletin de la Société Française de Minéralogie* 30: 326–455.
- Gatti, C., V. R. Saunders, and C. Roetti. 1994. "Crystal-Field Effects on the Topological Properties of the Electron-Density in Molecular Crystals - The Case of Urea." *Journal of Chemical Physics* 101: 10686–96.
- Groom, C. R., I. J. Bruno, M. P. Lightfoot, and S. C. Ward. 2016. "The Cambridge Structural Database." *Acta Crystallographica Section B: Structural Science, Crystal Engineering and Materials* 72: 171–79.
- Hegedus, B., and P. Zeller. 1965. "Di- or Tri-Hydroxybenzyl Hydrazides." United States Patent 3,178,476.
- Hirshfeld, F. L. 1977. "Bonded-Atom Fragments for Describing Molecular Charge Densities." *Theoretica Chimica Acta* 44: 129–38.
- Jokela, T., A. Salminen, and M. Hytönen. 2015. "Process for the Preparation of a Crystalline Polymorph of 2-Amino-3-Hydroxy-N'-(2,3,4-Trihydroxybenzyl)Propanehydrozide (Benserazide) Hydrochloride." International Patent Application WO 2015/197909 A1.
- Kabekkodu, S., A. Dosen, and T. N. Blanton. 2024. "PDF-5+ : A Comprehensive Powder Diffraction File™ for Materials Characterization." *Powder Diffraction* 39: 47–59.
- Kaduk, J. A., C. E. Crowder, K. Zhong, T. G. Fawcett, and M. R. Suchomel. 2014. "Crystal Structure of Atomoxetine Hydrochloride (Strattera), C₁₇H₂₂NOCl." *Powder Diffraction* 29: 269–73.
- Kresse, G., and J. Furthmüller. 1996. "Efficiency of Ab-Initio Total Energy Calculations for Metals and Semiconductors Using a Plane-Wave Basis Set." *Computational Materials Science* 6: 15–50.
- Leontowich, A. F. G., A. Gomez, B. Diaz Moreno, D. Muir, D. Spasyuk, G. King, J. W. Reid, C.-Y. Kim, and S. Kycia. 2021. "The Lower Energy Diffraction and Scattering Side-Bounce Beamline for Materials Science at the Canadian Light Source." *Journal of Synchrotron Radiation* 28: 1–9. doi:10.1107/S1600577521002496.
- Macrae, C. F., I. Sovago, S. J. Cottrell, P. T. A. Galek, P. McCabe, E. Pidcock, M. Platings, G. P. Shields, J. S. Stevens, M. Towler, and P. A. Wood. 2020. "Mercury 4.0: From Visualization to Design and Prediction." *Journal of Applied Crystallography* 53: 226–35.
- Materials Design. 2024. *MedeA 3.7.2*. Materials Design Inc.
- MDI. 2024. *JADE Pro Version 9.0*. Materials Data.
- Peintinger, M. F., D. Vilela Oliveira, and T. Bredow. 2013. "Consistent Gaussian Basis Sets of Triple-Zeta Valence with Polarization Quality for Solid-State Calculations." *Journal of Computational Chemistry* 34: 451–59.
- Rammohan, A., and J. A. Kaduk. 2018. "Crystal Structures of Alkali Metal (Group 1) Citrate Salts." *Acta Crystallographica Section B: Crystal Engineering and Materials* 74: 239–52.
- Silk Scientific. 2013. *UN-SCAN-IT 7.0*. Silk Scientific Corporation.
- Spackman, P. R., M. J. Turner, J. J. McKinnon, S. K. Wolff, D. J. Grimwood, D. Jayatilaka, and M. A. Spackman. 2021. "Crystalexplorer: A Program for Hirshfeld Surface Analysis, Visualization and Quantitative Analysis of Molecular Crystals." *Journal of Applied Crystallography* 54: 1006–11. doi:10.1107/S1600576721002910
- Stephens, P. W. 1999. "Phenomenological Model of Anisotropic Peak Broadening in Powder Diffraction." *Journal of Applied Crystallography* 32: 281–89.
- Sykes, R. A., P. McCabe, F. H. Allen, G. M. Battle, I. J. Bruno, and P. A. Wood. 2011. "New Software for Statistical Analysis of Cambridge Structural Database Data." *Journal of Applied Crystallography* 44: 882–86.
- Toby, B. H., and R. B. Von Dreele. 2013. "GSAS II: The Genesis of a Modern Open Source All Purpose Crystallography Software Package." *Journal of Applied Crystallography* 46: 544–49.
- van de Streek, J., and M. A. Neumann. 2014. "Validation of Molecular Crystal Structures from Powder Diffraction Data with Dispersion-Corrected Density Functional Theory (DFT-D)." *Acta Crystallographica Section B: Structural Science, Crystal Engineering and Materials* 70: 1020–32.
- Wavefunction, Inc. 2023. *Spartan '24. V. 1.0.0*. Wavefunction Inc.
- Wheatley, A. M., and J. A. Kaduk. 2019. "Crystal Structures of Ammonium Citrates." *Powder Diffraction* 34: 35–43.